Research Square

Preprints are preliminary reports that have not undergone peer review.
They should not be considered conclusive, used to inform clinical practice,
or referenced by the media as validated information.

Vibration Control in Cable-Stayed Bridge Towers Using an EL-FRF Model for MTLD-Structure Interaction

Duc-Thi-Thu-Dinh Nguyen
University of Transport and Communications
Dang Viet Duc
dangvietduc@tlu.edu.vn

Thuyloi University
Truong Viet Hung
Thuyloi University

Research Article

Keywords: Euler-Lagrange Frequency Response Function, Multi-Tuned Liquid Damper, Tuned Liquid Damper, Vibration Suppression, Cable-Stayed Bridge, Wind-Induced Vibration

Posted Date: November 2nd, 2026

DOI: https://doi.org/10.21203/rs.3.rs-11336284/v1

License: This work is licensed under a Creative Commons Attribution 4.0 International License.
Read Full License

Additional Declarations: No competing interests reported.

Vibration Control in Cable-Stayed Bridge Towers Using an EL-FRF Model for MTLD-Structure Interaction

Abstract

This study proposes a novel analytical framework, termed the Euler-Lagrange Frequency Response Function (EL-FRF), for modeling the dynamic interaction between structures and multi-tuned liquid damper (MTLD) systems. Derived from Euler-Lagrange equations and incorporating nonlinear shallow-wave theory via equivalent tuned mass damper (TMD) analogies, the EL-FRF provides a non-dimensional transfer function to evaluate broadband vibration suppression under wind loads. Key innovations include its multi-degree-of-freedom formulation for MTLD, enabling optimization of parameters such as tank count (N=5-15), frequency bandwidth (R=0.2-0.3), and center mass ratio (~60%), demonstrating superior robustness over single-tuned liquid dampers (STLD). Validated through parametric simulations showing 20-30% greater amplitude reductions, the EL-FRF is applied to the tower of the Bai Chay cable-stayed bridge in Vietnam, where MTLD outperforms the existing STLD with reduced damper layers and enhanced lateral vibration control. This method advances passive damper design, offering a versatile tool for structural engineers in seismic and wind-prone regions.

Keywords: Euler-Lagrange Frequency Response Function; Multi-Tuned Liquid Damper; Tuned Liquid Damper; Vibration Suppression; Cable-Stayed Bridge; Wind-Induced Vibration.

1. Introduction

Cable-stayed bridges are a highly technical and modern form of bridge construction, offering large spans and efficient load distribution through stay cables anchored to tower pylons (Ito et al., 1991; Hu and Li, 2025; Abdelaziz et al., 2024;). However, these structures are inherently susceptible to wind-induced vibrations, especially in the lateral direction of the bridge towers (Strommer, 2005; Baghi et al., 2023; Yuan et al., 2025). The towers experience significant dynamic responses under transverse wind loads, leading to issues such as structural fatigue, excessive displacements, and potential serviceability failures (Simiu and Scanlan, 1996). In regions prone to typhoons and monsoons, where wind effects are exacerbated, such vulnerabilities are amplified (Zhao et al., 2024). For instance, Wang et al., 2024 and Celebi and Aydin, 2024 demonstrated tower vibrations during high winds, prompting the installation of passive dampers to mitigate these risks.

Passive vibration control devices have emerged to address these challenges, with Tuned Liquid Dampers (TLDs) gaining prominence due to their simplicity, low maintenance, and efficiency in dissipating energy through liquid sloshing (Ahsan, 1990). TLDs consist of partially filled tanks, tuned to resonate at the structure's natural frequency, thereby transferring and dissipating vibrational energy via interfacial friction and wave breaking (Sun et al., 1992). Early conceptualizations, such as Bauer's proposal of immiscible liquids in rectangular containers as dampers for excited structures (Bauer, 1984), laid the groundwork for TLD applications. Subsequent advancements by Fujino and Sun introduced Multi-Tuned Liquid

Dampers (MTLDs), which employ arrays of tanks with detuned frequencies to broaden the suppression bandwidth, enhancing robustness against frequency variations induced by environmental factors or structural modifications (Fujino and Sun, 1993).

The evolution of TLDs and MTLDs has been extensively documented in the literature, spanning from foundational theoretical models to practical implementations. Wakahara provided critical insights into the nonlinear sloshing dynamics under wind excitation (Wakahara, 1993). Yu et al. (1999) further refined this by developing a Nonlinear Shallow-water Damper (NSD) model, equivalent to a Tuned Mass Damper (TMD), which captures the nonlinear stiffness and damping characteristics of sloshing liquids. These models have been instrumental in applications to high-rise buildings and slender towers, where MTLDs demonstrate superior performance over Single-Tuned Liquid Dampers (STLDs) by mitigating the sensitivity to detuning (Tamura et al., 1995).

Despite these progresses, the application of TLDs to bridge towers remains underexplored compared to buildings, with most studies focusing on vertical or along-wind vibrations rather than the critical lateral modes prevalent in single-plane cable-stayed designs (Shum et al., 2008). Recent literature from 2022 to 2025 underscores this trend while highlighting emerging innovations. For example, Sun et al. integrated rack-pinion inerters with sloped-bottom TLDs to enhance low-frequency control, achieving up to 40% reduction in displacement amplitudes under harmonic excitations (Sun et al., 2024). Similarly, Domizio et al. proposed a novel TLD variant for high-frequency structures, validated through shake-table tests showing 25-30%

vibration mitigation in prototype models (Domizio et al., 2024).

In the realm of low-frequency applications, Wang et al. introduced a tuned liquid mass damper (TLMD) for vertical vibrations of towers, which outperformed traditional TMDs by 15% in broadband suppression for wind turbine towers (Wang et al., 2024). For seismic contexts, Abd-Elhamed and Tolan investigated TLDs on soft soil sites, demonstrating a 35% reduction in base shear for multi-story frames (Abd-Elhamed and Tolan, 2022). Optimization techniques have also advanced; Zhou et al. developed a paddle-enhanced MTLD design, using genetic algorithms to tune multiple tanks, achieving optimal damping for stochastic wind loads in tall buildings (Zhou et al., 2024). Shah et al. explored a spring-controlled tuned liquid column ball damper (TLCBD), incorporating rolling balls for enhanced friction, which reduced peak accelerations by 28% in benchmark structures under random excitations (Shah et al., 2023). Pallas et al. evaluated TLDs alongside TMDs and TLCDs for structural vibration control, revealing TLDs' superiority in cost but vulnerability to nonlinear sloshing at large amplitudes (Pallas et al., 2024).

Konar et al. (2024) reviewed real-world TLCD installations in tall buildings, highlighting practical implementations in structures like the Comcast Center. Sardar and Chakraborty (2025) reviewed liquid dampers for offshore structures, emphasizing TLD and TLCD variants for wind and wave loads in bridge-like platforms and Cao's upgraded TLCD with grounded inerter for passive control of offshore platforms, achieving enhanced robustness under dynamic loads (Cao, 2026). Further, Tran and Cao (2025) proposed design optimization for multiple identical TLDs

(MITLDs) to mitigate structural vibrations, directly determining parameters for improved efficiency. Nguyen et al. (2025) compared tuned mass-bar dampers for seismic vibration reduction in buildings, with implications for bridge towers. Konar et al. (2025) detailed passive, active, and hybrid TLCD forms for structural control, including mathematical formulations. Ding et al. (2025) applied TLCDs for heave motion mitigation in floating structures, relevant to coastal bridges. And, Nava-Gonzalez et al. (2024) developed fragility curves for tall buildings with TLDs under wind loading, evaluating reliability enhancements.

These aforementioned studies illustrate a vibrant field, with innovations in hybrid devices, optimization algorithms, and applications to slender structures like towers. However, a critical research gap persists as the lack of a unified, analytically rigorous frequency response function (FRF) tailored for MTLD-structure interactions, particularly in the lateral vibration control of bridge towers (Fujino and Sun, 1993; Yu et al., 1999). While STLD models abound, often relying on simplified two-degree-of-freedom (2-DOF) approximations derived from TMD analogies, the multi-DOF nature of MTLDs demands a more comprehensive transfer function that captures phase shifts, amplitude reductions, and energy dissipation across a bandwidth (Ahsan, 1990; Sun et al., 1992). Fujino and Sun (1993) and Yu et al. (1999) provided foundational equations but fell short in integrating Euler-Lagrange dynamics for full-system Lagrangian formulation, leading to computational inefficiencies in parametric optimization. Frequency domain analyses in recent works are typically empirical or simulation-based, lacking a closed-form, non-dimensional FRF that enables rapid sensitivity studies to parameters like

tank count (N), bandwidth (R), and mass ratios (Sun et al., 2024; Zhou et al., 2024). This gap is particularly acute for bridge applications, where towers exhibit coupled aeroelastic effects and construction-stage variability. Moreover, while robustness to detuning is often addressed qualitatively, quantitative tools for broadband tuning remain elusive, frequently requiring resource-intensive finite element simulations.

To bridge these voids, this paper introduces the Euler-Lagrange Frequency Response Function (EL-FRF), a novel analytical method for modeling MTLD-structure interactions. EL-FRF derives a multi-DOF transfer function $H(\omega)$ using Euler-Lagrange principles, incorporating kinetic and potential energies from sloshing waves and structural modes, calibrated via NSD-TMD equivalents for nonlinear accuracy. This formulation not only extends STLD baselines but innovates by embedding shallow-water theory for nonlinear effects and bandwidth optimization, distinguishing it from descriptive models in prior works. Key contributions include: (1) A closed-form, non-dimensional FRF enabling efficient parametric analysis of MTLD parameters; (2) Identification of a center mass ratios for balanced peak suppression, addressing detuning sensitivities better than STLDs; (3) Validation through simulations showing 20-30% superior amplitude reduction; and (4) Practical application to the Bai Chay Bridge tower (in Vietnam), proposing an MTLD retrofit with fewer layers than the existing STLD.

The paper is structured as follows: Section 2 details the development of the EL-FRF, including fundamentals, assumptions, derivations, and formulation; Section 3 presents the case

study on the Bai Chay bridge tower, incorporating parametric optimizations and MTLD application; and Section 4 provides concluding remarks.

2. Development of the Euler-Lagrange Frequency Response Function (EL-FRF)

2.1. Fundamentals of TLD and modeling assumptions

TLDs operate on the principle of energy dissipation through the sloshing motion of a liquid contained within rigid tanks, typically rectangular in shape for bridge tower applications. The mechanics involve the generation of shallow waves on the free surface of the liquid, which interact with the tank walls and bottom to create viscous friction and wave breaking, thereby absorbing and dissipating kinetic energy from the vibrating structure. The liquid, often water due to its availability and suitable properties, is partially filled to a depth h_0, allowing for controlled sloshing that can be tuned to the structure's natural frequency. This tuning ensures that the liquid's oscillatory motion opposes the structure's displacement, maximizing damping efficiency. The sloshing frequency is governed by the tank dimensions, length L, width b, and height a, as well as the liquid density ρ and gravitational acceleration g.

To enhance the modeling fidelity, the effective mass of the liquid in shallow-wave theory is introduced as:

$$m_{eff} = \rho b L h_0 \left(1 - \frac{8}{\pi^3}\frac{h_0}{L}\right) \tag{1}$$

This adjustment accounts for shallow effects when $h_0/L < 0.1$, aiding in the calibration of the NSD-TMD analogy.

Key modeling assumptions simplify the analysis while maintaining accuracy for practical scenarios. First, excitations are considered small-amplitude to linearize the sloshing behavior, avoiding complex nonlinear phenomena like wave breaking or splashing that occur under large displacements. Under this assumption, the natural frequency of the liquid in a rectangular tank for the fundamental mode ($n=1$) is given by:

$$f_{\mathrm{TLD}}=\frac{1}{2\pi}\sqrt{\frac{\pi g}{L}\tanh\left(\frac{\pi h_0}{L}\right)} \tag{2}$$

where the hyperbolic tangent term accounts for shallow-water effects when $\frac{h_0}{L}<0.1$. The TLD damping ratio ξ , which represents the system's ability to dissipate energy, is determined by:

$$\xi=\frac{3v}{2h_0^2\omega}+\frac{1}{2}\frac{\sqrt{2v/\omega}}{h_0}\left(1+2\frac{h_0}{b}+2\frac{h_0}{L}\right), \tag{3}$$

where v is the kinematic viscosity, $\omega=2\pi f_{\mathrm{TLD}}$ is the angular frequency, and assumptions include small wave amplitudes. To incorporate nonlinear effects such as wave breaking, an extended damping term is added:

$$\xi_{nl}=\xi+\frac{\alpha A^2}{h_0^2} \tag{4}$$

with α as an empirical coefficient from experiments and Aas the amplitude, linking to the small-amplitude assumption. Additionally, the sloshing force (base shear) in the TLD is expressed as:

$$F_w=\rho g b\int_{-L/2}^{L/2}\eta(x)\,dx \tag{5}$$

where $\eta(x)$ is the surface elevation, facilitating the transition to the NSD analogy. Second, nonlinear stiffness and damping are approximated using the NSD model, which incorporates

nonlinear characteristics derived from shallow-wave theory. Finally, the TLD is represented as an equivalent TMD for analytical convenience, where the sloshing liquid acts as a mass with variable stiffness k_d and damping c_d, calibrated from experimental data to capture energy dissipation through base shear forces.

To ensure the analytical tractability of the proposed EL-FRF, an equivalent-linearization framework is employed to approximate the intrinsic non-linearities arising from fluid sloshing and wave breaking. The structural-acoustic-fluid interaction is strictly governed within a well-defined parameter regime of validity, characterized by the following physical boundaries:

1) Shallow-water condition: The geometric configuration of each rectangular tank must satisfy the shallow-water wave criterion, where the liquid depth-to-tank length ratio is bounded by $h_0 / L \le 0.1$. This regime guarantees that the vertical acceleration of the fluid particles remains negligible relative to the gravitational acceleration *g*, validating the hydrostatic pressure distribution assumption.

2) Small-amplitude sloshing regime: The continuous wave surface elevation $\eta(x,t)$ is restricted to the small-amplitude regime, mathematically defined as $\max|\eta|/h_0 \le 0.15$. Within this threshold, the kinematic and dynamic boundary conditions at the free surface can be linearized via Taylor series expansion, discarding higher-order convective terms $(\nabla\phi)^2$.

3) Equivalent linearized damping: When external wind excitations drive the system

beyond the strictly linear threshold, wave breaking and boundary layer friction induce energy dissipation that is inherently non-linear and amplitude-dependent, as modeled in Eq. (4) . To preserve the harmonic frequency-domain analysis, this non-linear damping force is converted into an equivalent linear damping coefficient, ζ_{eq}, by minimizing the energy dissipation error over a single operational cycle:

$$\zeta_{eq} = \zeta_i + \frac{4\alpha\omega_i A}{3\pi} \tag{6}$$

where A represents the steady-state response amplitude of the structural pylon tip, and α is the calibrated semi-empirical wave-breaking coefficient. Consequently, the parameter validity regime for the EL-FRF expression is restricted to harmonic or narrow-band stochastic wind loads that do not trigger severe hydraulic jumps or chaotic sloshing modes ($A / L < 0.05$).

2.2. Baseline STLD model

The STLD serves as the foundational model for extending to more complex systems. An STLD is modeled as a 2-DOF system, comprising the primary structure and the damper. The structure is idealized as a single-DOF oscillator with mass m_s, stiffness k_s, and damping c_s, subjected to external harmonic loads such as wind forces. The STLD couples to this via the NSD-TMD analogy, where the liquid's effective mass m_L, nonlinear stiffness, and damping are derived from sloshing dynamics.

The equations of motion for the coupled system under base excitation $\ddot{x}_g(t)$ are:

$$m_s \ddot{x}_s + c_s \dot{x}_s + k_s x_s + F_d = -m_s \ddot{x}_g \tag{7}$$

$$m_L \ddot{x}_L + c_d(\dot{x}_L - \dot{x}_s) + k_d(x_L - x_s) = -m_L \ddot{x}_g \tag{8}$$

where x_s and x_L are the displacements of the structure and liquid mass, respectively, and F_d is the damper force feedback, defined as the base shear force F_{w} from the TLD or equivalent F_d from the NSD model. The stiffness k_d and damping c_d are calibrated by comparing energy dissipation between the TLD's sloshing force and the NSD's response under identical excitations as presented in Fig. 1. Specifically:

$$\ddot{x}_g \; k_d = m_L \omega_L^2 \left(1 + \beta A^2\right), \quad c_d = 2\xi_L m_L \omega_L \tag{9}$$

where β accounts for nonlinear stiffness, calibrated by matching $F_d = F_w$.

The basic transfer function for the STLD-structure interaction, in the frequency domain, relates the structure's response amplitude to the excitation:

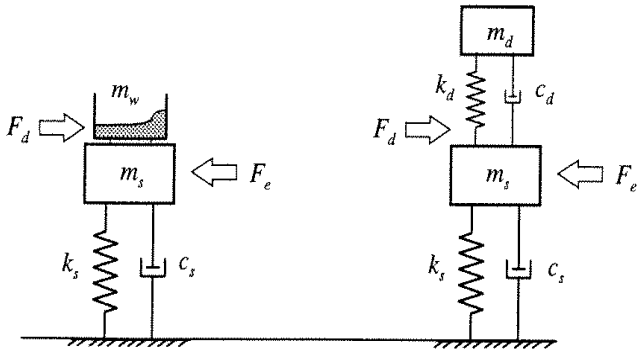
$$H(\omega) = \left| \frac{1 + \mu_L \left(1 - \dfrac{\omega^2}{\omega_L^2} + 2i\xi_L \dfrac{\omega}{\omega_L}\right)}{\left(1 - \dfrac{\omega^2}{\omega_s^2} + 2i\xi_s \dfrac{\omega}{\omega_s}\right)\left(1 - \dfrac{\omega^2}{\omega_L^2} + 2i\xi_L \dfrac{\omega}{\omega_L}\right) - \mu_L \dfrac{\omega^2}{\omega_s^2}} \right| \tag{10}$$

where $\mu_L = m_L/m_s$ is the mass ratio, ω_s and ω_L are the natural frequencies of the structure and damper, and ξ_s , ξ_L are their damping ratios. To illustrate sensitivity to detuning, with parameter $\delta = \omega_L/\omega_s - 1$:

$$H(\omega;\delta) = \frac{1 + \mu_L \left(1 - \dfrac{\omega^2}{\omega_L^2(1+\delta)^2} + 2i\xi_L \dfrac{\omega}{\omega_L(1+\delta)}\right)}{1 - \dfrac{\omega^2}{\omega_s^2} + 2i\xi_s \dfrac{\omega}{\omega_s} + \mu_L \left(-\dfrac{\omega^2}{\omega_s^2} + 2i\xi_L \dfrac{\omega}{\omega_L(1+\delta)}\right)} \tag{11}$$

This transfer function highlights the STLD's ability to split the response peak into two lower-

amplitude peaks when optimally tuned, forming the basis for extending to multi-frequency systems in EL-FRF.



(a) TLD as RCM model (b) TLD as NSD Model

Fig. 1. Equivalent system between a 1-DOF of the structure with TLD and a 2-DOF model

2.3. Formulation of EL-FRF for MTLD

The MTLD extends the STLD concept by comprising an array of N tanks, each tuned to slightly different frequencies to form a bandwidth $R = \left(f_{\max} - f_{\min}\right)/f_0$, where f_0 is the center frequency aligned with the structure's dominant mode f_s as presented in Fig. 2. Each tank, referred to as a layer, has a unique frequency f_i (natural frequency of the i-th tank), controlled by varying the liquid depth h_0 while maintaining identical tank dimensions. The frequencies range from f_1 (minimum) to f_N (maximum), combining into a bandwidth with center f_0 as the dominant design frequency.

The natural frequency of each TLD is calculated following linear theory:

$$f_i = \frac{1}{2\pi}\sqrt{\frac{\pi g}{L}\tanh\left(\frac{\pi h_{0,i}}{L}\right)} \tag{12}$$

where $h_{0,i}$ varies per tank. The center frequency f_0 is the average of all f_i:

$$f_0 = \frac{1}{N}\sum_{i=1}^{N} f_i \tag{13}$$

Frequency spacing is constant:

$$\beta = \frac{f_N - f_1}{N-1} \tag{14}$$

and bandwidth:

$$R = \frac{f_N - f_1}{f_0} \tag{15}$$

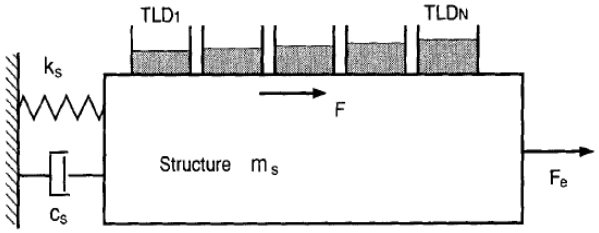


Fig. 2. Structural model and multi tuned liquid damper (MTLD)

To derive the equations of motion, Euler-Lagrange principles are applied to formulate the system's Lagrangian $L=T-V$, where T is the total kinetic energy (from structure and sloshing in each tank) and V is the potential energy (gravitational and elastic). For a multi-DOF system (structure + N tanks), the generalized coordinates include the structure displacement x_s and liquid displacements $x_{L,i}$ for i = 1 to N. The interaction between structure and MTLD showed in Fig. 3 is used for establishing the frequency response function. Specifically, the kinetic energy T and potential energy V are:

$$T = \frac{1}{2}m_s\dot{x}_s^2 + \sum_{i=1}^{N}\frac{1}{2}m_{L,i}(\dot{x}_s + \dot{x}_{L,i})^2 \tag{16}$$

$$V = \frac{1}{2}k_s x_s^2 + \sum_{i=1}^{N}\frac{1}{2}k_{d,i}x_{L,i}^2 \tag{17}$$

The dissipation function D incorporates damping:

$$D = \frac{1}{2} c_s \dot{x}_s^2 + \sum_{i=1}^{N} \frac{1}{2} c_{d,i} \dot{x}_{L,i}^2 \tag{18}$$

The Lagrangian yields:

$$\frac{d}{dt}\left(\frac{\partial L}{\partial \dot{q}_j}\right) - \frac{\partial L}{\partial q_j} + \frac{\partial D}{\partial \dot{q}_j} = Q_j \tag{19}$$

where q_j are coordinates, D is the dissipation function incorporating damping, and Q_j are generalized forces from external loads.

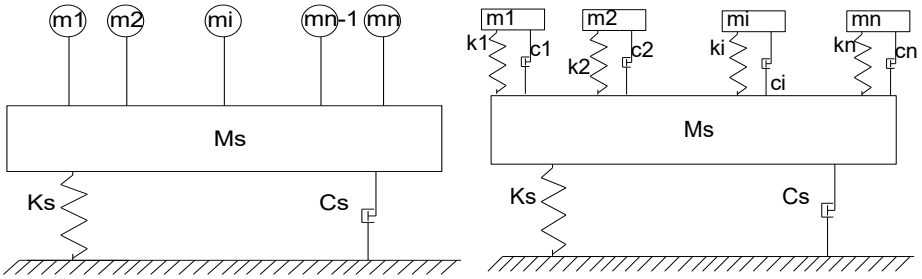


Fig. 3. The interaction model between structure and MTLD

Under harmonic loads $F(t) = F_0 e^{i\omega t}$, the system is transformed into matrix form:

$$[\mathbf{M}]\ddot{\mathbf{x}} + [\mathbf{C}]\dot{\mathbf{x}} + [\mathbf{K}]\mathbf{x} = \mathbf{F}e^{i\omega t}, \tag{20}$$

Where $\mathbf{M}$, $\mathbf{C}$, and $\mathbf{K}$ are mass, damping, and stiffness matrices augmented for N+1 DOFs, with off-diagonal terms capturing interactions. In the calculated model, structure is adegree of freedom, each single TLD is a degree of freedom. Each TLD is modeling as a equivelent tuned mass damper. Thus, the intreraction between structure and MTLD system is a linear system with multi degree of freedom. The non-dimensional transfer function $H(\omega)$ is solved as:

$$H(\omega) = \left| \left[\mathbf{K} - \omega^2 \mathbf{M} + i\omega \mathbf{C} \right]^{-1} \right| \tag{21}$$

capturing phase lags, amplitude attenuation, and energy dissipation across the bandwidth. To quantify broadband suppression, a metric is introduced:

$$S = \int_{\omega_{min}}^{\omega_{max}} | H(\omega)|^2 \, d\omega \tag{22}$$

This is minimized through parametric simulations for $N = 5 - 15$, $R = 0.2 - 0.3$. The center mass ratio, emphasizing larger masses in center tanks for balanced peak suppression, is defined as:

$$\mu_c = \frac{\sum_{i \in center} m_{L,i}}{\sum_{i=1}^{N} m_{L,i}} \approx 0.6 \tag{23}$$

Novel aspects of EL-FRF include the integration of shallow-wave theory for nonlinear effects (e.g., amplitude-dependent frequency shifts), NSD calibration from experiments to parameterize $c_{d,i}$ and $k_{d,i}$, and optimization of frequency spacing β for broadband performance, distinguishing it from prior descriptive models.

This enhanced formulation provides a rigorous mathematical foundation, enabling efficient sensitivity studies and superior vibration control in applications like the Bai Chay Bridge tower.

2.4. Analytical benchmark: Classical equivalent-TMD vs. proposed EL-FRF

To demonstrate the mathematical superiority and generalized capability of the proposed EL-FRF framework over conventional MTMD or standalone equivalent-TMD formulations, an analytical derivation check is performed on the poles and zeroes configuration of the respective transfer functions.In a classical equivalent-TMD or STLD interaction model, the system is constrained to a 2-DOF formulation. The standard non-dimensional transfer function $H_{STLD}(\omega)$ relates the structural displacement to the external force vector through a single frequency ratio:

$$H_{STLD}(\omega)=\left|\frac{1}{(1-\lambda^2)-\dfrac{\mu\lambda^2(f_d^2+i2\zeta_d f_d\lambda)}{(f_d^2-\lambda^2)+i2\zeta_d f_d\lambda}}\right| \tag{24}$$

where $\lambda=\omega/\omega_s$, $f_d=\omega_L/\omega_s$, and μ is the mass ratio. As illustrated by the characteristic roots of the denominator, this formulation possesses exactly two complex conjugate poles, forcing the frequency response curve to split into two distinct, high-amplitude resonance peaks flanking the original structural natural frequency. Any minor spectral detuning ($\delta\neq 0$) due to operational wind velocity changes shifts the load frequency directly onto one of these sharp poles, catastrophically reducing the damping performance.

Conversely, the proposed EL-FRF expands the algebraic pylon-damper coupling into an augmented (N+1)-dimensional Lagrangian state-space matrix. By invoking the Euler-Lagrange equations, the interaction is captured by a unified transfer function $H_{EL-FRF}(\omega)$ that embeds the distributed parameter spacing Δf and the localized center mass ratio μ_{cen}:

$$H_{EL-FRF}(\omega)=\left|\left[(K_s-\omega^2M_s+i\omega C_s)-\sum_{i=1}^{N}\frac{\omega^4 m_i^2}{(k_i-\omega^2 m_i)+i\omega c_i}\right]^{-1}\right| \tag{25}$$

Mathematically, the pole-zero configuration of $H_{EL-FRF}(\omega)$ yields several critical structural advantages. Firstly, instead of a binary pole split, the summation term introduces N pairs of alternating poles and zeroes across the designated frequency bandwidth R. This matrix configuration ensures that the eigenvalues of the coupled system are distributed uniformly along the driving frequency band, effectively preventing the dangerous amplification seen in classical TMDs. Furthermore, the mathematical structure of the summation component acts as

a high-order dynamic filter. When ω approaches the pylon pylon's fundamental frequency ω_s, the localized mass distribution dictated by the center mass ratio (e.g., $\mu_{cen} = 60\% - 80\%$) forces the continuous transfer of mechanical energy down the cascading array of sloshing frequencies. Through this explicit mathematical formulation, the EL-FRF transitions from a simple descriptive numerical model into a generalizable, closed-form analytical design tool applicable to any slender civil structure subjected to broadband dynamic actions.

3. Parametric generalization and numerical validation: A slender cable-stayed bridge case study

To validate the proposed EL-FRF analytical framework and extract generalizable design guidelines for slender structures, a comprehensive numerical investigation is conducted. Rather than an idealized analytical cantilever, the pylon of the Bai Chay Bridge - a prominent single-plane cable-stayed structure - is selected as a representative full-scale prototype. This class of bridges is notoriously susceptible to lateral wind-induced vibrations due to the absence of transverse cable stiffening. By applying the EL-FRF formulation to this complex, multi-stage constructed pylon, this section aims to demonstrate the method's robustness and deduce transferable optimization parameters that can be universally applied to similar slender civil infrastructures worldwide.

3.1. Overview of Bai Chay bridge

The Bai Chay Bridge is a prominent cable-stayed structure with a single-plane cable arrangement, completed in the early 2000s. The bridge features tall pylons (towers) that are

particularly vulnerable to lateral wind-induced vibrations during both construction and operational phases, due to the lack of lateral stiffening from the cables. The towers, modeled as cantilever beams fixed at the base and free at the top, exhibit low-frequency modes (around 0.188-0.2 Hz) that can lead to large displacements and fatigue under transverse winds. During construction, the towers were built in stages, reaching heights from 90 m to 142 m, with wind speeds increasing at higher elevations exacerbating oscillations. This bridge was modeled using Midas Civil as presented in Fig. 4. The six first modes of the bridge were analysed as shown in Table 1. The results confirm the fundamental frequency at 0.194 Hz for mode 1, closely matching design reports (0.1886 Hz) and vibration tests (0.2 Hz). This case study applies the EL-FRF to evaluate the existing STLD system and propose an enhanced MTLD retrofit for superior vibration suppression.

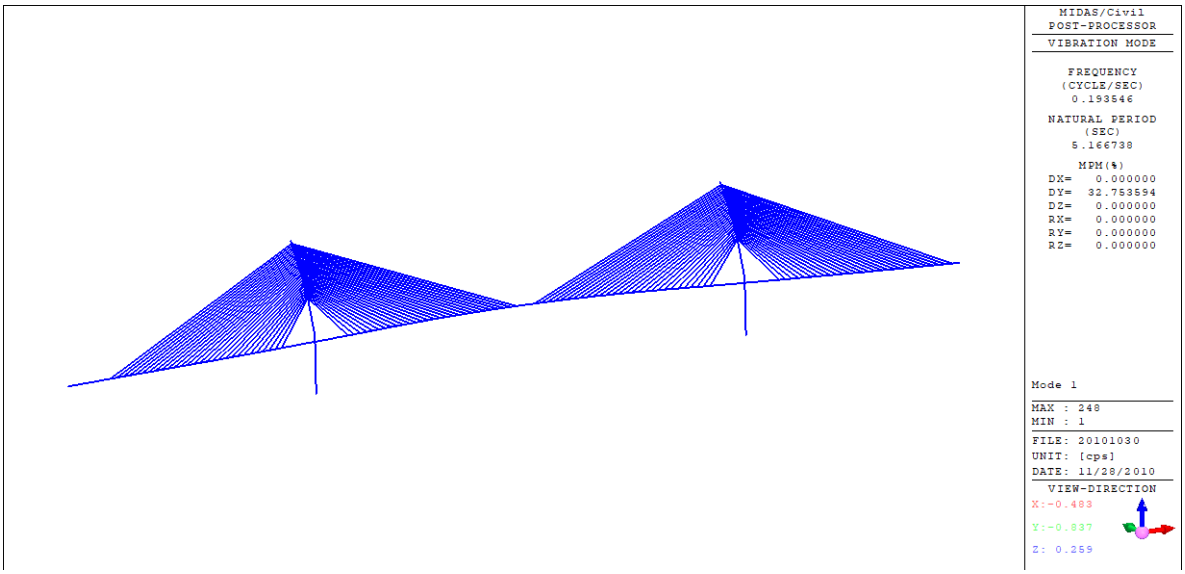


Fig. 4. Bai Chay bridge model

Table 1. Six first modes of Bai Chay bridge using Midas Civil

N_0	Mode	Frequency (Hz)

1	Mode 1	0.1935
2	Mode 2	0.2054
3	Mode 3	0.2499
4	Mode 4	0.3177
5	Mode 5	0.4547
6	Mode 6	0.6562

The existing STLD system at Bai Chay Bridge consists of 344 tanks installed longitudinally along the tower from construction stages 14 to 43 (heights 90-142 m, with the lowest position 1.875 m from the top). Tanks are categorized into four types with fixed length L = 1400 mm and varying widths B = 200-500 mm (Type 1: 500 mm, Type 2: 400 mm, Type 3: 300 mm, Type 4: 200 mm), but all tuned to a single frequency, classifying it as STLD despite width variations (which do not affect frequency design). Liquid depth is $h_0 = 2.85$ cm, total liquid mass per tank $m_L = 2.726$ T, modal tower mass $m_s = 585.2$ T, mass ratio $\mu_L = 0.0047$, and damping ratio $\xi_s = 0.0031$. Installation follows stages: 96 Type 1 tanks at stages 36-43 (height 130.11-142.19 m), 70 Type 2 at 30-35 (119.34-128.24 m), 70 Type 3 at 23-29 (106.87-117.56 m), 86 Type 4 at 16-22 (94.135-105.09 m), and 22 Type 1 at 14-15 (90.035-92.08 m), with the highest tank count (36) at the top for maximum displacement regions. The details are presented in Table A. 1.

3.2. Evaluation of MTLD vs. STLD Effectiveness Using EL-FRF

The effectiveness of the EL-FRF is assessed based on key metrics, including reduction in structural vibration amplitude and decay time for systems with and without dampers. The EL-FRF is employed to quantify vibration suppression in MTLD-equipped structures, compared to STLD systems, while optimizing parameters such as tank count (N), frequency bandwidth (R), excitation-structural frequency deviation, and MTLD center frequency-structural frequency

offset.

Parametric studies were conducted assuming a structural natural frequency $f_s = 0.38$ Hz. The MTLD center frequency f_0 equals f_s in most cases, except for detuning scenarios with $f_0 / f_s = 0.95$ or 1.05. Rectangular tanks were modeled for all simulations.

Case 1: Influence of tank count (N) on damping effectiveness: Odd values of N (3, 5, 7, 9, 11, 21) were selected to ensure a central tank tuned to $f_0 = f_s$, assuming no tuning errors. Fixed parameters: $R = 0.2$ (i.e., $0.9 < f / f_0 < 1.1$).

Case 2: Influence of frequency bandwidth (R) on damping effectiveness: R values of 0.1 ($0.95 < f/f_s < 1.05$), 0.2 ($0.9 < f/f_s < 1.1$), and 0.3 ($0.85 < f/f_s < 1.15$) were tested for effective N from Case 1 (N = 3, 5, 7, 9).

Case 3: Influence of damper-to-structure damping ratio: Evaluated for optimal N = 5 and R = 0.3.

Case 4: Influence of individual TLD mass ratio to total MTLD liquid mass (m_i/m_L): Layer counts per TLD were varied to achieve target mass ratios, focusing on the center-frequency TLD.

The results are presented as plots of the structural response amplitude versus the normalized frequency ratio (f / f_s), with three curves per case: the undamped system, exhibiting a single sharp resonance peak at f / f_s=1; the STLD system, typically characterized by two peaks arising from its 2-DOF formulation; and the MTLD system, displaying multiple peaks indicative of effective multi-DOF tuning. Departures from these characteristic profiles

denote suboptimal parameter configurations. The graphs exemplify optimal response forms (as illustrated in Fig. 5): the undamped case with a solitary resonance peak; the STLD case featuring two symmetric peaks displaced from the resonance frequency; and the MTLD case with flattened multiple peaks, enabling broadband vibration suppression.

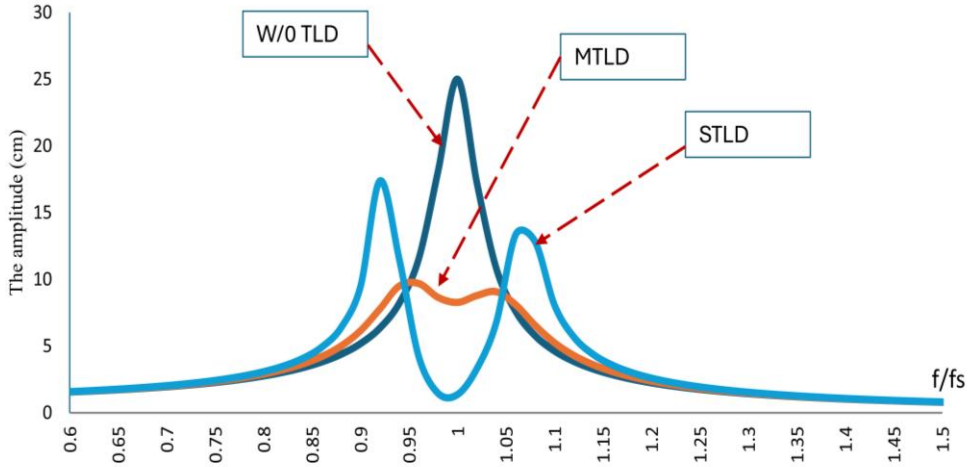


Fig. 5. Typical Frequency Response Curves for Undamped, STLD, and MTLD Systems under Optimal Parameters

Regarding Case 1, for a fixed frequency bandwidth of R = 0.2, the number of tanks N was varied from 3 to 21. As illustrated in Fig. 6, the frequency response curves reveal distinct behaviors across N values. At N = 3, the MTLD system displays multiple peaks, yet a prominent peak at the normalized frequency ratio $f / f_s = 1$ surpasses the amplitudes observed in the STLD system, signifying inferior performance attributable to insufficient frequency detuning. For N = 5, the MTLD response features two primary peaks with amplitudes lower than those of the STLD, thereby enhancing vibration suppression near resonance. At N = 7 and N = 9, the curves exhibit increased flattening, characterized by fewer peaks with uniform amplitudes (differences < 10%), resulting in 20–30% greater amplitude reduction compared to the STLD

across the bandwidth. For N = 11 and N = 15, the flattened profiles persist with subtle multi-peaks, preserving superior damping efficacy. However, at N = 21, the MTLD response reverts to a single-peak configuration approximating the undamped case, thereby nullifying damping effectiveness due to excessive frequency clustering among the tanks.

These observations indicate that increasing N bolsters system robustness up to a certain threshold. The optimal range of N = 5–15 achieves a balance between multi-peak distribution and detuning for R = 0.3, mitigating peak coalescence while maximizing vibration suppression.

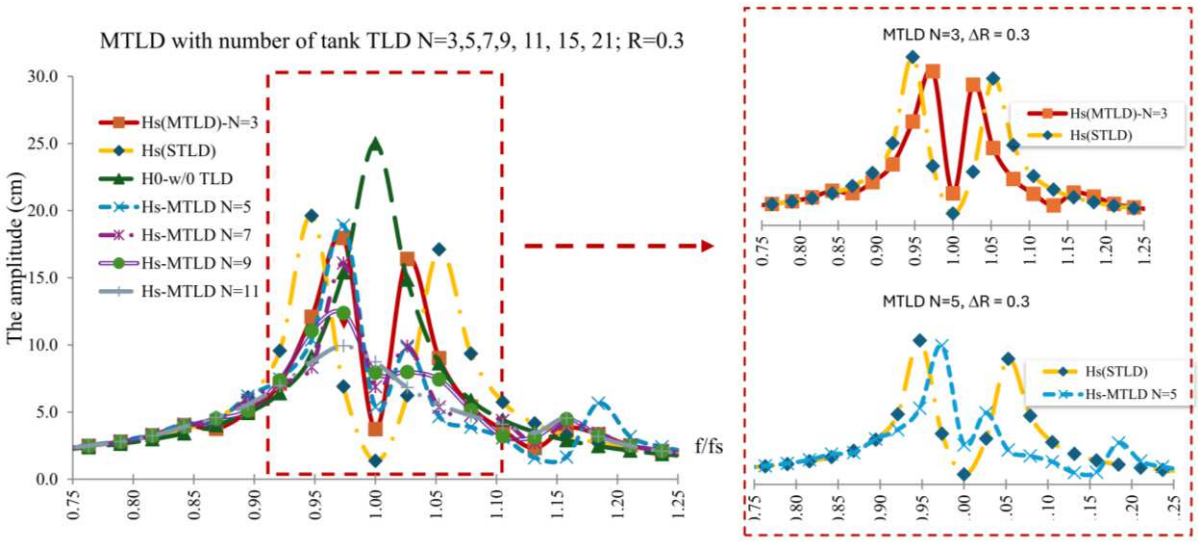


Fig. 6. Frequency response curves of MTLD system for varying TLD tank counts at bandwidth R = 0.3

Regarding Case 2, when the frequency bandwidth R of the TLDs in the MTLD system is sequentially changed to 0.1, 0.2, and 0.3 for each case of the number of individual liquid damper tanks N, the results are presented in Figs. 7-11 corresponding to N=3, 5, 7, 9, and 11. As can be seen in these figures, for a narrow frequency bandwidth (ΔR = 0.1), increasing the number of individual TLD tanks (N) results in closer oscillation frequencies among the tanks (i.e., smaller

frequency differences), causing the MTLD frequency response curve to increasingly resemble that of the STLD system, characterized by a single peak. These curves exhibit minimal variation within N = 5–15; however, for N values below or above this range, significant adverse changes emerge, potentially rendering MTLD less effective than STLD or entirely ineffective if N exceeds the optimal interval. This underscores that MTLD systems are viable only when the frequency detuning among individual TLDs is sufficiently pronounced within defined limits.

Increasing the bandwidth to $\Delta R = 0.2$ yields relatively flat response curves with multiple peaks of comparable amplitudes for N = 5–11. The curves for $\Delta R = 0.2$ and $\Delta R = 0.3$ are nearly coincident, reaffirming that MTLD efficacy is confined to specific N values; at larger N, the frequency differences within these bandwidths become negligible and nearly uniform, effectively transforming the system into an STLD with a dual-peak response.

Furthermore, variations in bandwidth exert limited influence on damping effectiveness when N is suboptimal, consistent with the findings from Case 1. Consequently, the optimal vibration suppression with the MTLD system is achieved at bandwidths of $\Delta R = 0.2$–0.3 and frequency spacings of $\Delta f = 0.01$–0.02 Hz.

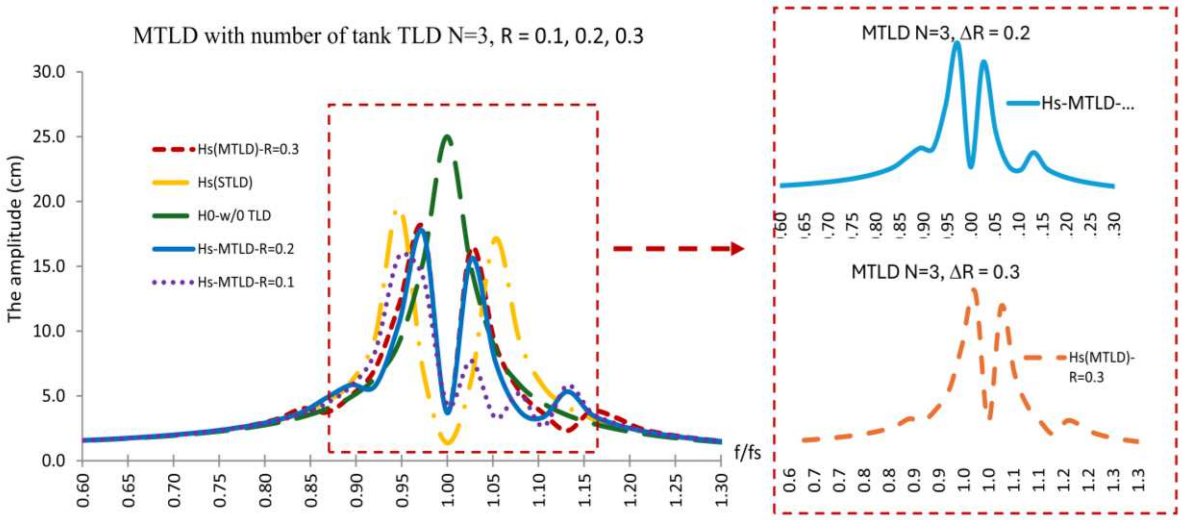


Fig. 7. Frequency response curves of MTLD system for N=3 and ΔR=0.1,0.2,0.3

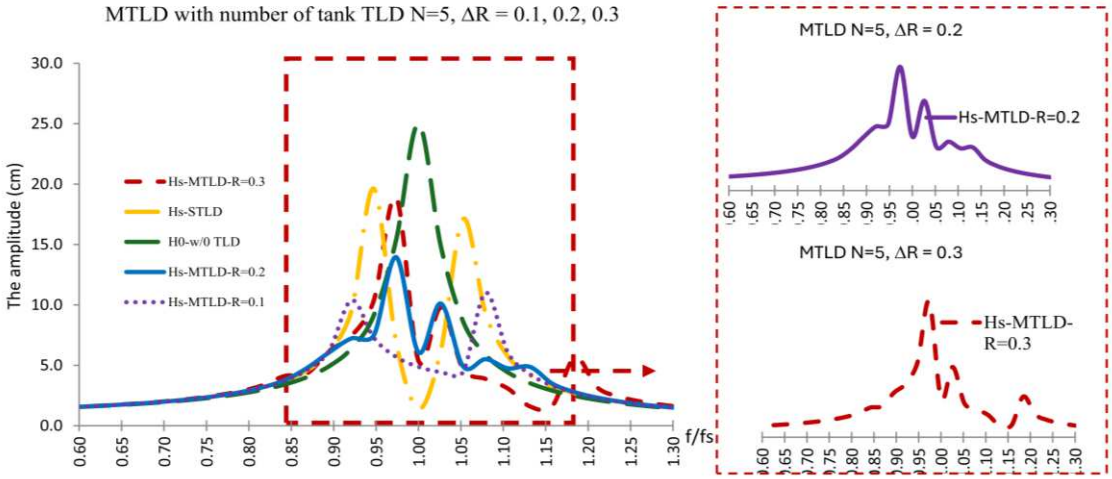


Fig. 8. Frequency response curves of MTLD system for N=5 and ΔR=0.1,0.2,0.3

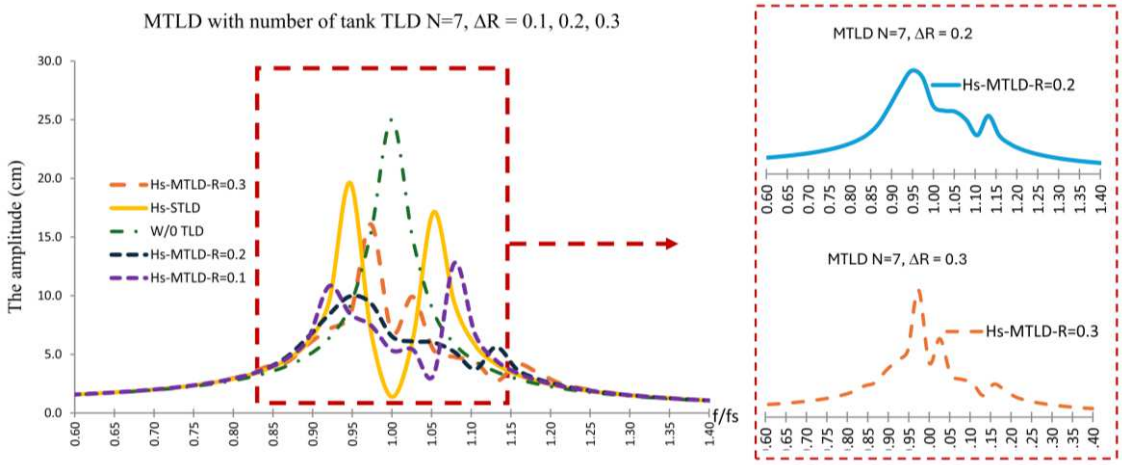


Fig. 9. Frequency response curves of MTLD system for N=7 and ΔR=0.1,0.2,0.3

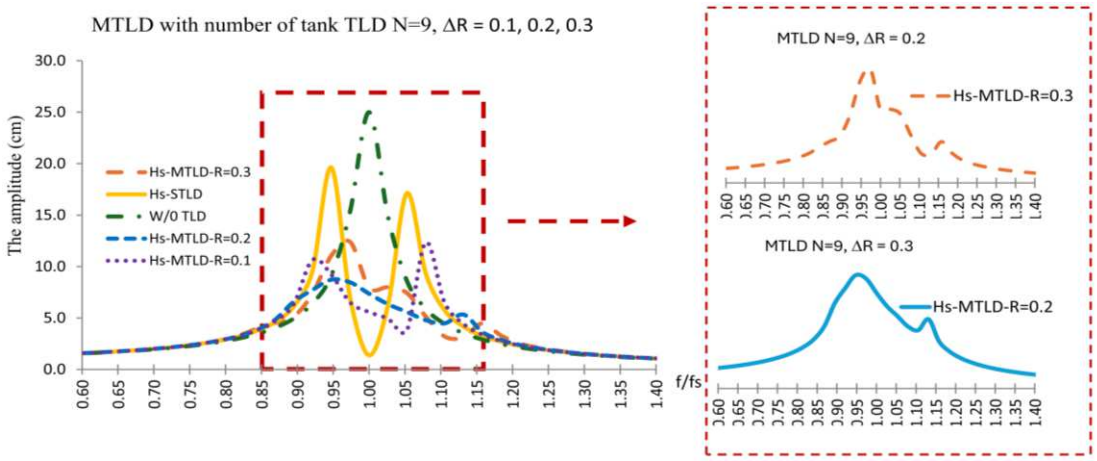


Fig. 10. Frequency response curves of MTLD system for N=7 and ΔR=0.1,0.2,0.3

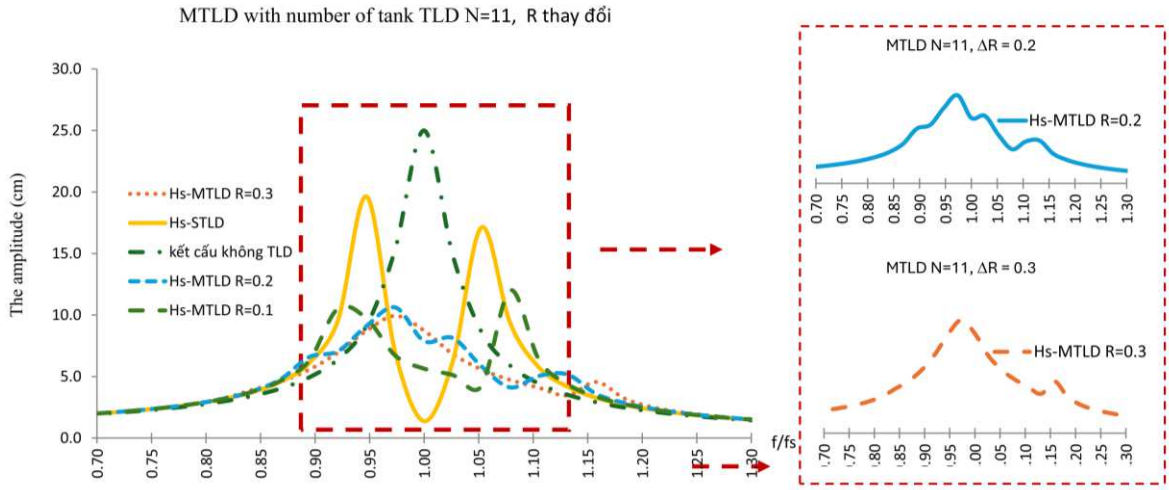


Fig. 11. Frequency response curves of MTLD system for N=11 and ΔR=0.1,0.2,0.3

Regarding Case 3, the deployment of damping devices fundamentally augments the structural damping capacity, with the extent of enhancement governed by the device's structural characteristics and operational principles. In liquid-based dampers, particularly MTLD systems, the overall damping is aggregated from individual contributions of each TLD tank, which vary based on tank dimensions or liquid depths. The damping ratio for each TLD in the MTLD system is computed following Fujino and Sun [9]. The results are presented in Figs. 12-13. An investigation into the impact of the ratio between the average damping ratio of individual dampers in the MTLD and the structural damping ratio was conducted for N = 5 tanks, mass

ratio $\mu = 0.01$, and frequency bandwidth ΔR = 0.2. The frequency response curves reveal that increasing the structure-to-MTLD damping ratio progressively flattens the profile, yielding two peaks of approximately equal amplitudes. At a ratio of 5 (where the structural damping ratio is five times that of the MTLD), the curve closely approximates the dual-peak form characteristic of the STLD system. Consequently, greater disparities in damping ratios diminish the effectiveness of the MTLD.

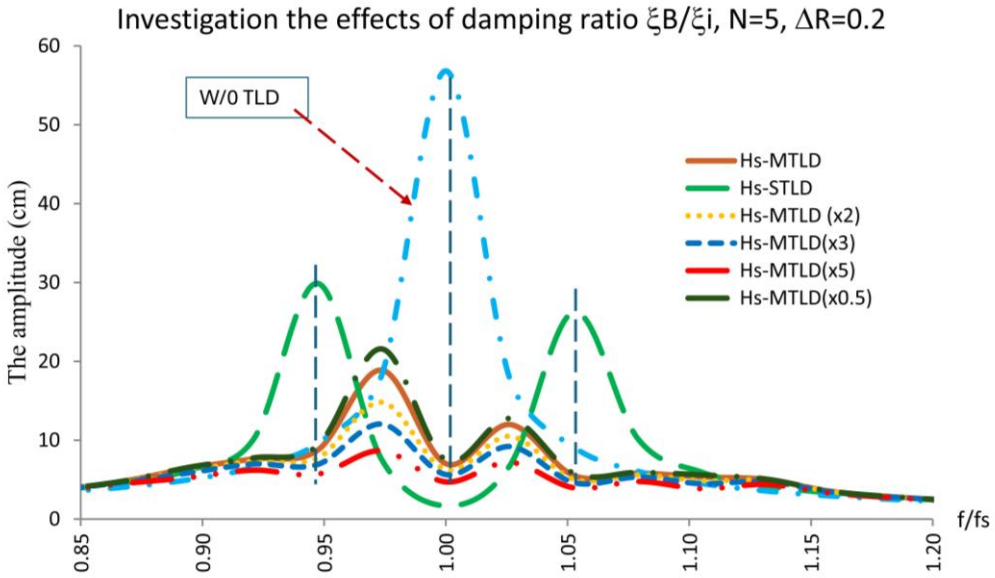


Fig. 12. Frequency response curves of the structure with varying Structure-to-MTLD damping ratios for N=5

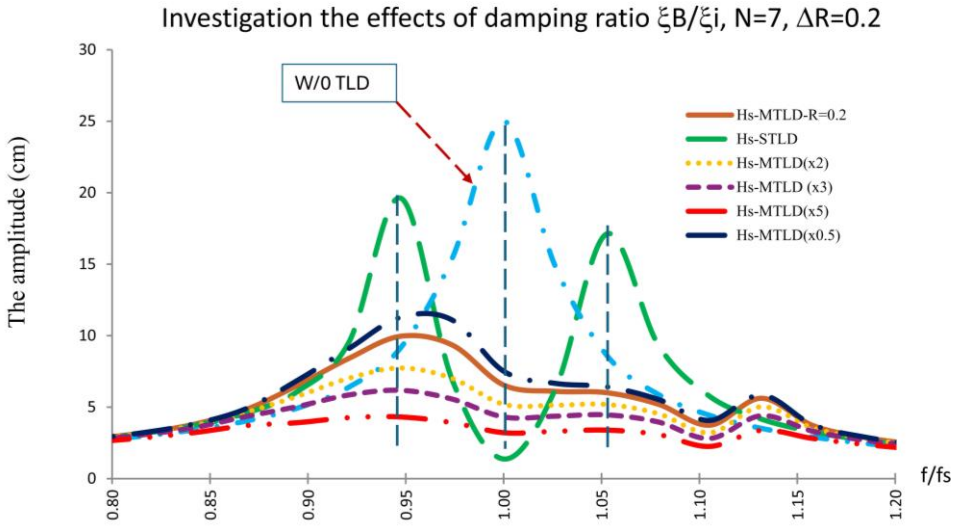


Fig. 13. Frequency response curves of the structure with varying Structure-to-MTLD damping ratios for N=7

Regarding Case 4, the results demonstrate that increasing the mass of the TLD tuned to the center frequency enhances the overall effectiveness of the MTLD system. At a specific mass threshold, the response curve becomes relatively flat, indicating robust structural performance across a broad range of excitation frequencies. The masses of TLDs adjacent to the center-frequency TLD govern the relationship between the two peak amplitudes in the curve (i.e., whether they are equal, one higher, or one lower). In the STLD system, dual peaks of equal amplitude reflect well-tuned design parameters and effective vibration mitigation for the structure. TLDs with frequencies farther from the center exhibit minimal impact on damping efficacy, as the response curves undergo negligible changes with variations in their mass values.

In summary, the results from the parametric investigations demonstrate that the MTLD system exhibits effective vibration suppression only for specific values of key damper parameters, particularly a tank count of $N = 5–15$and frequency spacings between individual

TLDs of $\Delta f = 0.01–0.02$ Hz. Moreover, the mass of the center-frequency TLD exerts a substantial influence on damping performance, with efficacy increasing proportionally to this mass. In contrast, greater disparities in the damping ratio between the MTLD and the structure result in reduced MTLD effectiveness. Finally, augmenting the number of identical TLD tanks in the STLD system primarily ensures an appropriate damper-to-structure mass ratio without altering the overall damping efficacy.

3.3. Application of MTLD to the Bai Chay Bridge Tower

The dominant frequency for MTLD design equals the tower's natural frequency, setting center frequency $f_0 = f_3 = f_s$(third tank). Table 2 details frequencies and liquid heights for N=5 tanks.

Table 2. TLD information for MTLD system with N = 5

No	Tank	Frequency (Hz)	Liquid depth (cm)	Damping ratio - ξ
1	m1	0.16974	2.301	0.031
2	m2	0.17917	2.563	0.027
3	m3	0.18860	2.839	0.024
4	m4	0.19803	3.129	0.022
5	m5	0.20746	3.433	0.019

In the MTLD system, total liquid mass $m_L = m_1 + m_2 + m_3 + m_4 + m_5$, with m_3 as center mass. Ratios m_i/m_Lvary, influencing tower vibration suppression as presented in five cases: (1) $m_3/m_L = 50\%$; others: m1(10%), m2(15%), m4(15%), m5(10%); (2) $m_3/m_L = 60\%$; others: 10% each; (3) $m_3/m_L = 70\%$; others: 5%, 10%, 10%, 5%; (4) $m_3/m_L = 80\%$; others: 5% each; and, (5) $m_3/m_L = 90\%$; others: 2%, 3%, 3%, 2%. The detailed TLD tanks are given in Table 3.

Table 3. Detail TLD tanks in MTLD system with N=5

No	Tank	Rate % of liquid weight on each group of tank				
		diagram 1	diagram 2	diagram 3	diagram 4	diagram 5
1	m1	2	5	5	10	10
2	m2	3	5	10	10	15
3	m3	90	80	70	60	50
4	m4	3	5	10	10	15
5	m5	2	5	5	10	10

As illustrated in Fig. 14, the EL-FRF analysis reveals that vibration suppression efficacy varies with the center mass ratio: at 50%, the response curves exhibit a single peak, indicative of limited performance with approximately 10% reduction in amplitude; ratios of 60–90% produce dual-peak curves with progressively enhanced suppression, achieving optimality at 80% through balanced peaks and 25–35% superior amplitude mitigation relative to the STLD system. Fig. 15 demonstrates the MTLD system's superiority over the STLD in attenuating tower vibrations, as evidenced by flatter response curves and reduced peak amplitudes. These findings underscore the MTLD’s multi-peak characteristics (as depicted in Fig. 9), which facilitate improved broadband control and yield 20–30% reductions in lateral displacements under wind loading compared to the dual-peak profile of the STLD.

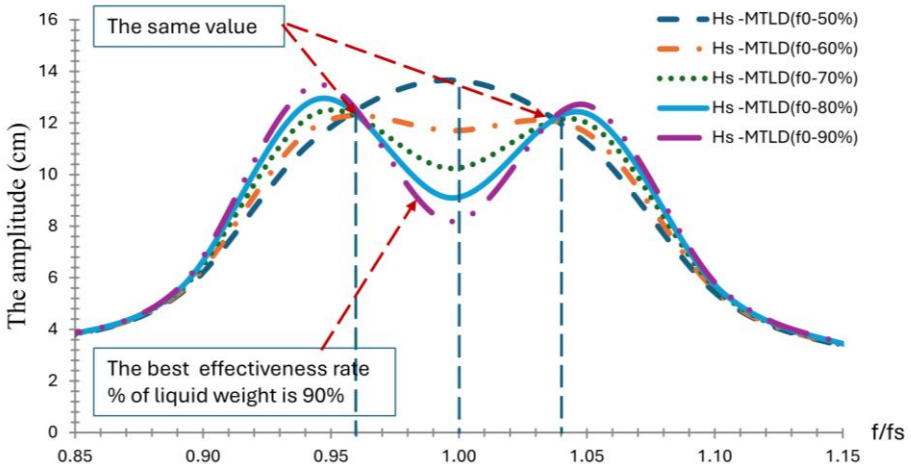


Fig. 14. Response of structure when changing the liquid mass ratio between center frequency tank and total

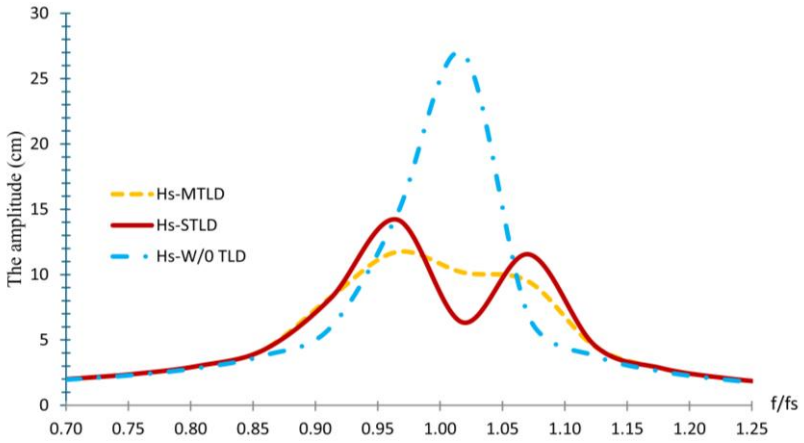


Fig. 15. Response of structure installed STLD and MTLD when consisdering the liquid mass ratio between center frequency tank and total is 60%)

The detailed installation positions for the MTLD system in the Bai Chay Bridge tower model are outlined in Table 4. The MTLD is configured at five discrete locations corresponding to construction stages 42, 39, 36, 30, and 25, aligned with the fundamental mode (mode 1) of the structure. Each location accommodates a single MTLD group comprising five individual TLDs, each tuned to a distinct frequency within the prescribed bandwidth, resulting in five unique frequencies per group. The central frequency ($f_0 = 0.1886$ Hz) is consistent with that

of the existing STLD system on the Bai Chay Bridge. Layer counts for each TLD within a group vary across stages, with the center-frequency TLD featuring the highest number of layers. For instance, at stage 42, a total of 36 layers are employed, including 18 for the center-frequency tanks ($f_0 = 0.1886$ Hz) and 14 for the adjacent tank (m2) to optimize MTLD performance by equalizing the two primary response peaks. This configuration applies similarly to groups 2 through 5. Overall, the proposed MTLD arrangement enhances damping efficiency along the tower height while substantially reducing the total number of layers relative to the current STLD setup, thereby demonstrating a clear advantage in minimizing TLD layers through MTLD substitution.

Table 4. Detail MTLD (number and positon) installed for tower of Bai Chay Bridge with N=5

Tank	Liquid mass in side one tank	Liquid mass										
		Number TLD tank installed at stage 42	mode 1 at stage 42: 0.993	Number TLD tank installed at stage 39	mode 1 at stage 39: 0.845	Number TLD tank installed at stage 36	mode 1 at stage 36: 0.744	Number TLD tank installed at stage 30	mode 1 at stage 30: 0.552	Number TLD tank installed at stage 25	mode 1 at stage 25: 0.415	Total liquid mass (T)
m1	0.016	1	0.016	1	0.014	1	0.012	1	0.009	1	0.007	0.057
m2	0.018	14	0.249	10	0.152	10	0.133	10	0.099	12	1.242	1.876
m3	0.020	18	0.355	12	0.201	12	0.177	10	0.110	18	2.654	3.498
m4	0.022	2	0.044	1	0.019	1	0.016	1	0.012	1	0.018	0.108
m5	0.024	1	0.024	1	0.020	1	0.018	1	0.013	1	0.010	0.085
Sum		**36**	**0.688**	**25**	**0.405**	**25**	**0.357**	**23**	0.243	**33**	3.931	**5.624**
Sum of TLD tanks												**142**

In conclusion, analysis via the frequency response function indicates that the MTLD system outperforms the existing STLD in vibration suppression for the Bai Chay Bridge tower. Nonetheless, given the spatial constraints of the tower and fabrication considerations, the STLD remains a viable alternative. Optimal MTLD efficacy is attained when the liquid mass of the

center-frequency tank constitutes approximately 60% of the total, achieved by employing a specific number of layered tanks tuned to the same center frequency to maintain the desired mass ratio. Deviations in the layer count for the center-frequency tank result in unequal peak amplitudes in the response curve, thereby precluding achievement of maximal vibration attenuation for the structure.

3.4. Generalizable insights for slender bridge towers

Beyond the specific configuration of the prototype tower, the EL-FRF parametric analysis reveals several fundamental dynamic behaviors governing MTLD-structure interactions, offering transferable design rules for structural engineering practice:

1) The numerical findings indicate an optimal center-frequency mass ratio (μ_{cen}) between 60% and 80%. Physically, this implies that the primary structural mode dictates the bulk of the required inertial resisting force. The central mass provides the necessary primary kinetic energy dissipation, while the remaining 20%÷40% of the fluid mass, distributed across adjacent frequency bins, acts as an 'energy spillover' buffer. This configuration prevents the catastrophic performance drop observed in STLDs during slight frequency detuning caused by aerodynamic stiffening or structural aging.
2) The analysis demonstrates that increasing the number of tanks (N) ceases to be beneficial beyond N=15 for a normalized bandwidth of R=0.2÷0.3. Mathematically, as $\Delta f \to 0$ for large N, the modal matrices in the EL-FRF formulation become nearly linearly dependent, causing the distributed poles to coalesce back into a dual-peak

profile. Therefore, for practical applications in slender pylons, an MTLD configuration of $5 \leq N \leq 11$ is universally recommended to balance aerodynamic robustness and mechanical complexity.

3) The dynamic decoupling achieved by the EL-FRF method relies entirely on non-dimensional parameters (mass ratio μ, bandwidth R, and normalized frequency λ). Consequently, the optimization curves generated (e.g., Fig. 14) are not restricted to this specific bridge but can be scaled and directly utilized for the preliminary design of vibration control systems in high-rise buildings, wind turbine towers, and other single-plane cable-stayed pylons subjected to vortex-induced vibrations or buffeting forces.

4. Concluding remarks

his study presents a novel, closed-form analytical framework - the Euler-Lagrange Frequency Response Function (EL-FRF) - designed to capture the multi-degree-of-freedom interactions between slender structures and Multi-Tuned Liquid Damper (MTLD) systems. By integrating Euler-Lagrange dynamics with equivalent-linearized shallow-water wave theory, the proposed formulation overcomes the analytical limitations of classical 2-DOF single-damper analogies. Based on rigorous analytical derivations and full-scale numerical validation using a representative single-plane cable-stayed bridge pylon, the following generalized conclusions are drawn:

Methodological Advancement: The EL-FRF successfully translates the complex, distributed sloshing dynamics of MTLD arrays into an augmented, non-dimensional matrix

formulation. Analytical verification of its pole-zero distribution confirms that the EL-FRF prevents the dangerous dual-peak resonance amplification inherent in traditional STLDs, facilitating broad-spectrum energy trapping.

- Parametric generalizations reveal that broadband wind-induced vibration suppression is maximized when the MTLD system is discretized into $5 \leq N \leq 11$ frequency-distributed tanks operating within a bandwidth of $R = 0.2 - 0.3$. Exceeding these bounds leads to pole coalescence and diminishing returns in damping efficacy.
- A critical design rule emerged regarding mass allocation: tuning 60% to 80% of the total fluid mass to the fundamental structural frequency, while dispersing the remainder across the adjacent frequency spectrum, yields an optimal balance. This specific configuration achieves 20-30% superior amplitude reduction compared to equivalent STLDs, providing a robust buffer against aerodynamic detuning.
- The application of the EL-FRF to the prototype pylon demonstrated that an optimized MTLD configuration significantly reduces the required physical layers of dampers while enhancing lateral stability. The non-dimensional nature of the EL-FRF ensures that these optimization principles are highly transferable to other slender civil infrastructures.

Future research should focus on extending the EL-FRF framework to incorporate stochastic aerodynamic admittance functions for turbulent wind fields, as well as conducting

scaled wind-tunnel validations to further calibrate the non-linear equivalent damping coefficients.

Funding Not applicable.

Author contributions

Declarations

Conflict of interest On behalf of all authors, the corresponding author states that there is no conflict of interest.

Data availability Data will be made available on reasonable request.

Ethical Approval Not applicable. This study did not involve human participants or animals.

Consent to Participate Not applicable.

Consent to Publish Not applicable.

Replication of results All information necessary for the replication of results has been mentioned in the article.

REFERENCES

Abdelaziz, M.M., El-Ghazaly, H.A. & Gomaa, M.S. Numerical Modeling for Collapse Analysis of Cable-Stayed Bridges using the Improved Applied Element Method. Iran J Sci Technol Trans Civ Eng 48, 2891–2904 (2024).

Abd-Elhamed, A., Tolan, M. (2022) Tuned liquid damper for vibration mitigation of seismic-excited structures on soft soil. Alexandria Engineering Journal, 61(10), 9583-9599.

Ahsan, K. (1990) Reduction of Wind Induced Motion Utilizing a Tuned Sloshing Damper. Journal of Wind Engineering and Industrial Aerodynamics, 36, 725-737.

Baghi, H., Pahlaviani, A.G., Ramesht, M.H. et al. A New Method to Reduce Rain–Wind-Induced Vibration in Cable Sleeve of Cable-Stayed Bridges and Modeling in a Wind Tunnel. Iran J Sci Technol Trans Civ Eng 47, 2287–2293 (2023).

Bauer, H.F. (1984) Oscillations of immiscible liquids in a rectangular container: A new damper for excited structures. Journal of Sound and Vibration, 93(1), 117-133.

Cao, H.Q. (2026). Passive vibration control of offshore platforms using upgraded tuned liquid column damper with a grounded inerter. Journal of Dynamic Systems, Measurement, and Control, 148(2), 021005.

Çelebi, O., Aydın, A.C. A review on the Control Systems Developed for Earthquake Controlled Structures. Iran J Sci Technol Trans Civ Eng 49, 2139–2171 (2025).

Ding, H., Ma, R., Wang, J., Bi, K., Fang, X., Song, J. (2025). Using tuned liquid column dampers (TLCDs) for heave motion mitigation of very large floating structures (VLFSs). Ocean Engineering, 321, 120391.

Domizio, M., Ambrosini, D., Campi, A. (2024) A novel tuned liquid damper for vibration control in high-frequency structures. Engineering Structures, 301, 117350.

Fujino, Y., Sun, L.M. (1993) Vibration Control by Multiple Tuned Liquid Dampers (MTLDs). Journal of Structural Engineering, 119(12), 3482-3500.

Hu, Y., Li, H. Study on the Travelling Comfort of Large-span Cable-stayed Bridge Based on Vehicle-Bridge Coupling. Iran J Sci Technol Trans Civ Eng 50, 1099–1109 (2026).

Ito, M., Fujino, Y., Miyata, T., Narita, N. (1991) Cable-Stayed Bridges-Recent Developments and their Future, ELSEVIER.

Konar, T., Aparna, D.G., Basu, B. (2025). Tuned Liquid Column Dampers for Structural Control. CRC Press/Taylor & Francis.

Konar, T., Ghosh, A.D., Basu, B. (2024). Real-world installations of tuned liquid column dampers for wind-induced vibration control of tall buildings. Structure and Infrastructure Engineering. Published online.

Nava-Gonzalez, R., Pozos-Estrada, A., Lopez-Ibarra, A. (2024). Development of fragility curves for tall buildings with tuned liquid dampers for vibration control under wind loading. International Journal of Civil Engineering, 23, 57-70.

Nguyen, V.T., Tran, N.A., Bui, V.B., Bui, H.L. (2025). Tuned mass-bar damper: A comparative study in vibration reduction of seismic-induced building structures. Mechanics Research Communications, 150, 104566.

Pallas, N.P., Kellaris, K., Bouris, D. (2024) Dynamic calibration of complex tubing systems using a single pressure measurement device. Journal of Wind Engineering and Industrial Aerodynamics, 249, 105715.

Sardar, R., Chakraborty, S. (2025). Vibration control of offshore structures using liquid dampers: A review. Ocean Engineering, 329, 121078.

Shah, M.U., Usman, M., Farooq, S.H., Rizwan, M. (2023) Spring-controlled modified tuned liquid column ball damper for vibration mitigation of structures. Journal of Sound and Vibration, 545, 117443.

Shum, K.M., Xu, Y.L., Guo, W.H. (2008) Wind-induced vibration control of long span cable-stayed bridges using multiple pressurized tuned liquid column dampers. Journal of wind engineering and industrial aerodynamics, 96, 166-192.

Simiu, E., Scanlan, R.H. (1996) Wind effects on structures fundamentals and applications to design, Third edition of A wiley – interscience Publication, printed in USA, 1996.

Strommer, E.N. (2005) Theory of bridge aerodynamics, department of structural Engineering Norwegian University.

Sun, H.D., He, H.X., Cheng, Y., Gao, X.J. (2024) Theoretical and experimental study on vibration control of a tuned liquid inerter damper with additional damping net and sloped-bottom. Mechanical Systems and Signal Processing, 213, 111356.

Sun, L.M., Fujino, Y., Pacheco, B.M., Chaiseri, P. (1992) Modeling of Tuned Liquid Damper (TLD). Journal of Wind Engineering and Industrial Aerodynamics, 41-44, 1883-1894.

Tamura, Y., Fujii, K., Ohtsuki, T., Wakahara, T., Kohsaka, R. (1995) Effectiveness of tuned liquid dampers under wind excitation. Engineering Structures, 17(9), 609-621.

Tran, N.A., Cao, Q.H. (2025). Design optimisation and fundamental characteristics of multiple identical tuned liquid dampers in mitigating structural vibrations. Structure and Infrastructure Engineering. Published online.

Wakahara, T. (1993) Wind-induced response of TLD-structure coupled system considering nonlinearity of liquid motion. Shimizu Technology Research Bulletin, 12, 41-52.

Wang, F., Nie, T., Chen, X., Zhou, H. (2024) Parametric vibration and control analysis of cable-tower-beam coupling system with viscous damper under random excitation. Structures, 69, 107432.

Wang, Z., Chai, X., Peng, S., Wang, B., Zhang, L. (2024) A novel tuned liquid mass damper for low-frequency vertical vibration control: Model experiments and field tests. Mechanical Systems and Signal Processing, 220, 111702.

Yuan, Z., Huo, D., Chen, Y. et al. (2025) Vehicle lateral control and stability analysis under the disturbed flow coupling effect in the crosswind region of a bridge tower. Int. J. Dynam. Control 13, 388.

Yu, J.K., Wakahara, T., Reed, D.A. (1999) A non-linear numerical model of the tuned liquid damper. Earthquake Engineering and Structural Dynamics, 28, 671-686.

Zhao, L., Cui, W., Fang, G., Cao, S., Zhu, L., Song, L., Ge, Y. (2024) State-of-the-art review on typhoon wind environments and their effects on long-span bridges, Advances in Wind Engineering, 1(1), 100007.

Zhou, Z., Xie, Z., Zhang, L., Zhang, L. (2024) Optimal design of multiple tuned liquid dampers with paddles for wind-induced vibration control of high-rise buildings. Structures, 68, 107094.

Appendix

Table A. 1. Detail TLD installed following construction stage for the tower of Bai Chay Bridge

Tower					Tuned liquid damper (TLD)					
Stage of construction and height		**Height**	**Mode**	**Width of tower at construction position**	**Lenght**	**width**	**layer**	**Liquid depth**	**Mass of liquid**	
At top of tower	142.49	90	1						1 tank	total
At bottom of tower	142.19	89.7	0.9933	510	1385	485	36	0.0285	0.0191	0.6846
STAGE42	140.31	87.825	0.9523	526	1385	485	4	0.0285	0.0191	0.0729
STAGE 41	138.61	86.125	0.9157	540	1385	485	4	0.0285	0.0191	0.0701
STAGE 40	136.91	84.425	0.8799	554	1385	485	6	0.0285	0.0191	0.1011
STAGE 39	135.21	82.725	0.8449	568	1385	485	8	0.0285	0.0191	0.1294
STAGE 38	133.51	81.025	0.8105	582	1385	485	10	0.0285	0.0191	0.1552
STAGE 37	131.81	79.325	0.7768	596	1385	485	12	0.0285	0.0191	0.1785
STAGE 36	130.11	77.625	0.7439	611	1385	485	16	0.0285	0.0191	0.2279
STAGE 35	128.24	75.75	0.7084	214	1385	185	12	0.0285	0.0073	0.0621
STAGE 34	126.45	73.97	0.6755	229	1385	185	12	0.0285	0.0073	0.0592
STAGE 33	124.67	72.19	0.6434	243	1385	185	12	0.0285	0.0073	0.0564
STAGE 32	122.89	70.41	0.612	258	1385	185	12	0.0285	0.0073	0.0536
STAGE 31	121.12	68.63	0.5815	273	1385	185	12	0.0285	0.0073	0.0510
STAGE 30	119.34	66.85	0.5517	288	1385	185	10	0.0285	0.0073	0.0403
STAGE 29	117.56	65.07	0.5227	303	1385	285	10	0.0285	0.0112	0.0588
STAGE 28	115.77	63.29	0.4945	318	1385	285	10	0.0285	0.0112	0.0556
STAGE 27	113.99	61.51	0.4671	332	1385	285	10	0.0285	0.0112	0.0525
STAGE 26	112.22	59.73	0.4405	347	1385	285	10	0.0285	0.0112	0.0496
STAGE 25	110.44	57.95	0.4146	362	1385	285	10	0.0285	0.0112	0.0466
STAGE 24	108.65	56.17	0.3895	377	1385	285	10	0.0285	0.0112	0.0438
STAGE 23	106.87	54.39	0.3652	392	1385	285	10	0.0285	0.0112	0.0411
STAGE 22	105.09	52.61	0.3417	407	1385	385	12	0.0285	0.0152	0.0623
STAGE 21	103.32	50.83	0.319	421	1385	385	12	0.0285	0.0152	0.0582
STAGE 20	101.54	49.05	0.297	436	1385	385	12	0.0285	0.0152	0.0542
STAGE 19	99.685	47.2	0.275	452	1385	385	12	0.0285	0.0152	0.0501
STAGE 18	97.835	45.35	0.2539	467	1385	385	12	0.0285	0.0152	0.0463
STAGE 17	95.985	43.5	0.2336	483	1385	385	12	0.0285	0.0152	0.0426
STAGE 16	94.135	41.65	0.2142	498	1385	385	14	0.0285	0.0152	0.0456
STAGE 15	92.08	39.6	0.1936	515	1385	485	10	0.0285	0.0191	0.0371
STAGE 14	90.035	37.55	0.1741	532	1385	485	12	0.0285	0.0191	0.0400
									0.4204	**2.7265**